Adsorption 5, 419–433 (1999)

Backfill Cycle of a Layered Bed H_2 PSA Process

HYUNGWOONG AHN AND CHANG-HA LEE
Department of Chemical Engineering, Yonsei University, Shinchon-dong, Seodaemun-gu, Seoul, 120-749, Korea
leech@bubble.yonsei.ac.kr

BONGKOOK SEO, JAEYOUNG YANG AND KIHWANG BAEK
R&D Tech. Center, Sunkyong Engineering & Construction, Seoul, 110-300, Korea

Received September 30, 1998; Revised February 16, 1999; Accepted April 2, 1999

Abstract. The backfill cycle of two-bed PSA process using activated carbon beds, zeolite 5A beds, and layered beds was studied experimentally and theoretically to recover high purity H_2 from coke oven gas. In a layered bed PSA, a comparison was made between two PSA processes with/without a backfill step before the feed pressurization step. Since the backfill step made the adsorption bed rich in H_2 and this led to a rather steep concentration wave front at the feed pressurization step, incorporating a backfill step resulted in an increase in product purity with a decrease in recovery. Each step of the single-adsorbent and layered bed PSA processes with a backfill step was simulated with a dynamic model incorporating mass, energy, and momentum balances. The model agreed well with the experimental results in predicting the product H_2 purity and recovery, thus giving a basic understanding of the bed dynamics of a backfill cycle. While the concentration and temperature profiles of a layered bed in each step showed characteristic behavior of each adsorbent in each layer, the product purity of a layered bed was not between the limits of two single-adsorbent bed processes. The concentration profiles predicted by simulation showed that CO and N_2 played an important role in obtaining high H_2 purity.

Keywords: backfill step, single-adsorbent bed, layered bed, coke oven gas, H_2 PSA

Introduction

There has been a tremendous growth in pressure swing adsorption (PSA) during the past three decades through the modification of established processes and the development of new adsorbents. Thus, PSA is currently used to separate a wide range of gas mixtures, and the largest plants are those built for H_2 purification. In the H_2 PSA process, many versions of the process incorporating three to twelve adsorption beds had been developed for 99.99–99.9999% H_2 purity with 70–90% recovery (Yang, 1987; Ruthven et al., 1994). The high purity and recovery of the H_2 PSA processes are largely due to the innovative and effective operation of multibed PSA processes including several pressure equalizations, product pressurization, backfill, and layered adsorption beds.

When only one gas component is being recovered, commercial units favor the backfill step to supplement the feed gas mixture. This is because it is a much simpler and cheaper process than using a portion of product gas. However, to obtain a high purity product, the backfill step involves the pressurization of the adsorption bed with the product in a direction opposite to that of the feed gas mixture. Skarstrom (1963) used the product to repressurize the bed in a PSA process separating H_2 from hydrocarbons using activated carbon. Kirkby and Kenney (1987) carried out equilibrium modeling and experimental studies on the backfill step showing that there was no clear optimum backfill pressure above

0.53 ratio of the backfill pressure to feed pressure. They also pointed out that the simultaneous use of the backfill and purge steps gave high product recovery and purity. This indicates that it would therefore be possible for the backfill step to maintain product purity and recovery when pressurization and product release steps are combined. The backfill step with a light product in a zeolite 5A oxygen PSA process under the isothermal condition was studied by Liow and Kenney (1990). In their study, the effect of the backfill pressure ranging from purge pressure to adsorption pressure was investigated by a two-bed PSA process without pressure equalization and purge steps. This study showed that, after a rapid increase of oxygen concentration with increasing backfill pressure, the oxygen concentration does not vary much with backfill pressure. This backfill step or product pressurization step has commercially been used to increase product purity (Chou and Huang, 1994).

The important characteristic of the H_2 PSA process is that many different adsorbents are used either through using multiple-layered beds or through incorporating two groups of adsorption beds with different adsorbents. The typical layered beds used in commercial H_2 PSA have a carbon layer and a zeolite layer, while a guard layer can also be located under the carbon layer in order to prevent the detrimental impurities from entering the main bed. Recently, Yang and Lee (1998) studied the adsorption dynamics of a layered bed using coke oven gas (COG) through breakthrough experiments and non-isothermal dynamic model. Although the initial conditions were different, Yang et al. (1998) also pointed out that the concentration profiles in the layered bed PSA were very similar to those of the breakthrough experiments. However, in spite of the wide utilization of a layered bed with a backfill step in a commercial H_2 PSA, there are very few works which have studied the influence of the backfill step in a layered bed PSA.

In this study, the two-bed PSA process for high purity H_2 recovery from COG which consists of H_2, CH_4, CO, CO_2, and N_2 was studied experimentally and theoretically. By using a layered bed, a seven-step PSA process with a backfill step was compared with a conventional six-step PSA process without a backfill step. The experimental results were analyzed numerically by using a non-isothermal dynamic model incorporating mass, energy, and momentum balances. Furthermore, to understand the role of the backfill step in single-adsorbent and layered PSA processes, the dynamic behavior of each step in these three different beds was also compared through model simulation.

PSA Process Description

Two kinds of PSA processes with/without a backfill step were employed to obtain high purity hydrogen from COG. A typical six-step two-bed PSA process goes through the following steps: (I) feed pressurization (FP), (II) high-pressure adsorption (AD), (III) depressurizing pressure equalization (DPE), (IV) countercurrent depressurization (DP), (V) purge with a light product (PG), and (VI) pressurizing pressure equalization (PPE). The cycle sequence for the six-step process and a simple flow diagram were illustrated in Fig. 1(a). This PSA process was described elsewhere in detail (Yang et al., 1997a).

The other PSA process incorporated a backfill step (BF) as the seventh step into the above process as shown in Fig. 1(b). In this process, the feed pressurization step was divided into backfill and feed pressurization steps. During the backfill step, the adsorption bed was pressurized with a part of a light product from a product tank. And the backfill pressure was done up to the average pressure of the final pressure of pressure equalization step and the adsorption pressure. According to the pressurization method used in this PSA process, the bed is pressurized by a three-staged pressurization (pressurizing pressure equalization, backfill, and feed pressurization) like the four-bed PSA process (Kumar, 1994).

The effluent in step II, the high-pressure adsorption step, was a high-purity H_2 product. The product purity and recovery of a light component were used when separation performance of the two processes was compared. The step times of the two processes are also shown in Fig. 1. The combined step time of backfill and feed pressurization in the seven-step PSA process was set equal to the step time of feed pressurization in the six-step PSA process so that two different PSA processes had an identical total cycle time. The pressure equalization step time, 20 s, was determined from the previous work (Yang et al., 1997a).

Mathematical Modeling

A mathematical model including mass, energy, and momentum balances was constructed to develop a complete non-isothermal PSA model with the following assumptions: (i) the flow pattern is described by the

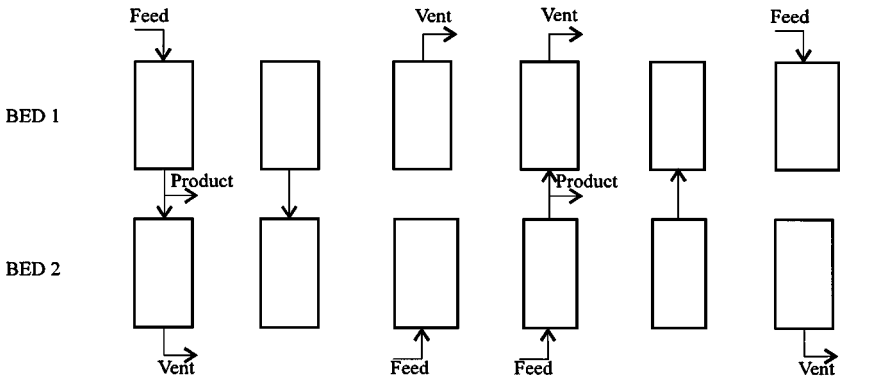

BED 1	AD(180)	DPE(20)	DP(8)	PG(180)	PPE(20)	FP(8)
BED 2	PG(180)	PPE(20)	FP(8)	AD(180)	DPE(20)	DP(8)

(a)

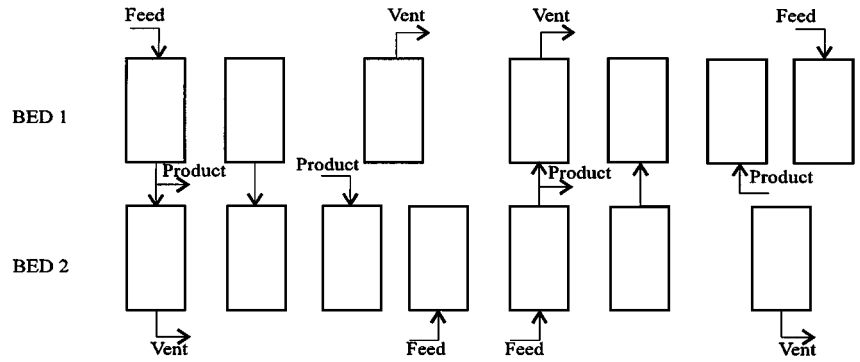

BED 1	AD(180 s)	DPE(20 s)	DP(8 s)		PG(180 s)	PPE(20 s)	BF(4 s)	FP(4 s)
BED 2	PG(180 s)	PPE(20 s)	BF(4 s)	FP(4 s)	AD(180 s)	DPE(20 s)	DP(8 s)	

(b)

AD , adsorption ; DPE , depressurizing pressure equalization ; DP , depressurization ;
PG , purge ; PPE , pressurizing pressure equalization ; BF , backfill ; FP , feed pressurization

Figure 1. Flow diagrams and cycle sequences of (a) a six-step and (b) a seven-step processes. (values in the parenthesis are step times.)

axially dispersed plug flow model, (ii) thermal equilibrium is assumed between fluid and particles, (iii) the mass transfer rate is represented by a linear driving force (LDF) model, (iv) the gas phase behaves as an ideal gas mixture, and (v) radial concentration and temperature gradients are negligible.

The material balance for the bulk phase in the adsorption column and the overall mass balance could be represented as follows:

$$-D_{\mathrm{L}}\frac{\partial^2 y_i}{\partial z^2}+\frac{\partial y_i}{\partial t}+u\frac{\partial y_i}{\partial z}+\frac{RT}{P}\frac{1-\varepsilon}{\varepsilon}\rho_{\mathrm{p}} \times\left(\frac{\partial \bar{q}_i}{\partial t}-y_i\sum_{j=1}^{n}\frac{\partial \bar{q}_j}{\partial t}\right)=0 \tag{1}$$

$$-D_{\mathrm{L}}\frac{\partial^2 P}{\partial z^2}+\frac{\partial P}{\partial t}+P\frac{\partial u}{\partial z}+u\frac{\partial P}{\partial z} +PT\left(-D_{\mathrm{L}}\frac{\partial^2}{\partial z^2}\left(\frac{1}{T}\right)+\frac{\partial}{\partial t}\left(\frac{1}{T}\right)+u\frac{\partial}{\partial z}\left(\frac{1}{T}\right)\right) -D_{\mathrm{L}}T\frac{\partial}{\partial z}\left(\frac{1}{T}\right)\frac{\partial P}{\partial z}+\frac{1-\varepsilon}{\varepsilon}\rho_{\mathrm{p}}RT\sum_{j=1}^{n}\frac{\partial \bar{q}_j}{\partial t}=0 \tag{2}$$

The energy balance for gas and solid phases was given by

$$-K_{\mathrm{L}}\frac{\partial^2 T}{\partial z^2}+(\alpha\rho_{\mathrm{g}}(C_{\mathrm{p}})_{\mathrm{g}}+\rho_{\mathrm{B}}(C_{\mathrm{p}})_{\mathrm{s}})\frac{\partial T}{\partial t} +\rho_{\mathrm{g}}(C_{\mathrm{p}})_{\mathrm{g}}\varepsilon u\frac{\partial T}{\partial z}-\rho_{\mathrm{B}}\sum_{i}^{n}Q_i\frac{\partial \bar{q}_i}{\partial t} +\frac{2h_i}{R_{\mathrm{B}_i}}(T-T_{\mathrm{w}})=0 \tag{3}$$

where K_{L} is the effective axial thermal conductivity (Suzuki, 1990).

Due to the small diameter of the adsorption bed used in the present study, another energy balance for the wall of the adsorption bed was used. However, the axial conductivity in the stainless steel wall was neglected because the wall axial conduction in this study was not significant in comparison with the heat amount caused by the heat of adsorption:

$$\rho_{\mathrm{w}}(C_{\mathrm{p}})_{\mathrm{w}}A_{\mathrm{w}}\frac{\partial T_{\mathrm{w}}}{\partial t}=2\pi R_{\mathrm{B}i}h_i(T-T_{\mathrm{w}}) -2\pi R_{\mathrm{B}o}h_o(T_{\mathrm{w}}-T_{\mathrm{atm}}) \tag{4a}$$

$$A_{\mathrm{w}}=\pi\left(R_{\mathrm{B}o}^2-R_{\mathrm{B}i}^2\right) \tag{4b}$$

The Ergun's equation was applied to the pressure drop across the bed (Lu et al., 1993; Alpay et al., 1993; Yang et al., 1998).

$$-\frac{dP}{dz}=a\mu\nu+b\rho\nu|\nu| \tag{5a}$$

$$a=\frac{150}{4R_{\mathrm{p}}^2}\frac{(1-\varepsilon)^2}{\varepsilon^3},\quad b=1.75\frac{(1-\varepsilon)}{2R_{\mathrm{p}}\varepsilon^3} \tag{5b}$$

where ν is superficial velocity.

The sorption rate into the adsorbent pellet was described by the following LDF model with a single lumped mass transfer parameter, ω (Ruthven et al., 1994; Hartzog and Sircar, 1995).

$$\frac{\partial \bar{q}_i}{\partial t}=\omega_i\left(q_i^*-\bar{q}_i\right) \tag{6}$$

The equilibrium of mixtures was predicted by following the extended Langmuir-Freundlich model:

$$q_i=\frac{q_{\mathrm{m}i}B_iP_i^{n_i}}{1+\sum_{j=1}^{n}B_jP_j^{n_j}} \tag{7a}$$

$$q_{\mathrm{m}}=k_1+k_2T,\quad B=k_3e^{k_4/T},\quad n=k_5+\frac{k_6}{T} \tag{7b}$$

The axial dispersion coefficient, D_{L}, in Eqs. (1) and (2) was calculated by a Wakao equation using interstitial feed velocity at the adsorption pressure and this constant value was used for all the steps (Wakao and Funazkri, 1978; Ruthven, 1984):

$$\frac{D_{\mathrm{L}}}{2uR_{\mathrm{p}}}=\frac{20}{ReSc}+0.5 \tag{8}$$

The effective axial thermal conductivity, K_{L}, in Eq. (3) was estimated by the following empirical correlation (Suzuki, 1990).

$$K_{\mathrm{L}}/k_{\mathrm{g}}=K_{\mathrm{L}0}/k_{\mathrm{g}}+\delta PrRe \tag{9a}$$

$$K_{\mathrm{L}0}/k_{\mathrm{g}}=\varepsilon+\frac{1-\varepsilon}{\phi+(2/3)(k_{\mathrm{g}}/k_{\mathrm{s}})} \tag{9b}$$

$$\phi=\phi_2+(\phi_1-\phi_2)\left(\frac{\varepsilon-0.26}{0.216}\right) \quad \text{for} \quad 0.260\le\varepsilon\le0.476 \tag{9c}$$

The well-known Danckwerts boundary conditions were applied to the steps which had influent streams. The boundary conditions and parameters used in the

PSA simulation were the same as the previous work (Yang and Lee, 1998).

To develop a mathematical model for a layered bed PSA process, the layered adsorption bed packed with zeolite 5A and activated carbon was assumed to be made of two independent beds with a single adsorbent in each bed. To express a packing ratio, the so-called carbon ratio was defined as a ratio of the activated carbon layer length to bed length. This mathematical model and numerical simulation for a layered bed PSA process were described elsewhere in details (Yang and Lee, 1998).

Experimental Study

The two-bed PSA system used in the present study, as shown in Fig. 2, consisted of two stainless steel columns of 100 cm in length and 3.71 cm in ID. The feed gas used as COG was the H_2 (56.4 vol%) mixture gas with CH_4 (26.6 vol%), CO (8.4 vol%), N_2 (5.5 vol%), and CO_2 (3.1 vol%). Zeolite 5A is almost saturated with CO_2 at low pressure, indicating that CO_2 is very difficult to desorb and thus gives a detrimental effect on zeolite 5A. In the feed gas, the activated carbon shows larger adsorption capacity based on the unit mass of the adsorbent than zeolite 5A except N_2 gas. Therefore, in a layered bed, the activated carbon (PCB: 6–16 mesh, Calgon Carbon Co.) was packed at the bottom of the column. On top of the carbon layer, zeolite 5A (4–8 mesh, W.R. Grace Co.) was packed after putting a metal screen with 0.3 mm thickness between two layers. The characteristics of the adsorption bed and adsorbents are listed in Table 1.

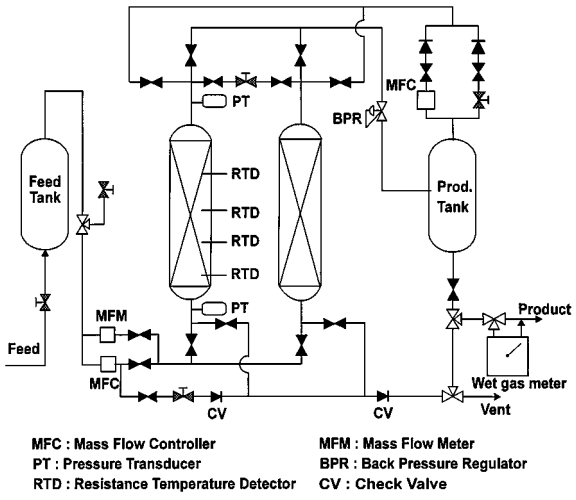

Figure 2. Schematic diagram of a two-bed PSA system.

Table 1. Characteristics of the adsorption bed and adsorbents.

	Activated carbon bed	Zeolite 5A bed
Adsorption bed		
Length	100 cm	100 cm
Inside diameter	3.71 cm	3.71 cm
Outside diameter	4.245 cm	4.245 cm
Heat capacity of wall	0.12 cal/(g K)	0.12 cal/(g K)
Bulk (bed) density	0.482 g/cm^3	0.764 g/cm^3
External void fraction	0.433	0.357
Total void fraction	0.78	0.77
Adsorbents		
Pellet size	4–8 mesh	6–16 mesh
Pellet density	0.85 g/cm^3	1.16 g/cm^3
Heat capacity	0.25 cal/(g K)	0.22 cal/(g K)

Feed and purge flow rates were controlled by mass flow controllers (Bronkhorst high-tech, F-201C). To calculate the recovery accurately, the amount of gas flowing into and out of the PSA system were measured with a mass flow meter (Bronkhorst high-tech, F-112ac-HA-55-V) and a wet gas meter (Shinagawa, W-NK-1B). The system was fully controlled by interfacing with a personal computer (PC) and a self-made control program. All the measured data including flow rate, pressure, and temperature were saved on the computer through an AD converter. Gas samples taken from the product tank were analyzed mainly by using a mass spectrometer (Balzers, QME 200) and these samples were also confirmed by GC (HP, GC 5890 II) using carboxen 1004 micropacked column supplied by Supelco.

The details are described in the previous work (Yang and Lee, 1998).

Results and Discussion

Effect of Backfill Step in a Layered Bed

As mentioned in the PSA process description, two kinds of layered bed PSA processes were examined in the present study. A major difference between two processes was the pressurization method up to the adsorption pressure. In the conventional six-step two-bed PSA process (Fig. 1(a)), the adsorption bed was pressurized through a two-staged pressurization, which was feed

pressurization after the pressurizing pressure equalization step (Yang et al., 1997a, 1997b). It is well known that light product pressurization improves light product purity and the purity of heavy product can be elevated by employing a cocurrent depressurization and/or a heavy product rinse step. This implies that product purity is affected mainly by a cyclic step as well as operating conditions. Therefore, to improve product purity by using two adsorption beds, the backfill step was employed (Fig. 1(b)).

The effects of feed rate on product purity and recovery in two different PSA processes are shown in Fig. 3(a) and (b). All the experimental and simulated results were obtained at 11 atm adsorption pressure and 0.7 LSTP/min purge rate using a layered bed with 0.35 carbon ratio. The results showed that the seven-step PSA process was better than the six-step PSA process with respect to product purity. However, as for product purity, the seven-step process began to lose its advantage at low feed rate. The reason was that, even in the six-step PSA process, the product end section was kept clean in the range of low feed rate by keeping the concentration wave fronts far from the product end. Consequently, the need to make the product end section clean by a countercurrent backfill was reduced. For recovery, the seven-step process was worse than the six-step process under the flow rate below 10 LSTP/min because some amount of light product was consumed during the backfill step. On the other hand, the recovery difference between the two processes decreased with an increase in the feed rate and the simulated results showed a crossover of recovery above 10 LSTP/min feed rate. Since lower purity in the adsorption step means less amount of H_2 in a product, this might be responsible for the crossover in H_2 recovery between the two processes. Fig. 3(c) shows productivity in the range of the experimental feed rates. The productivity of the six-step PSA was higher than that of the seven-step PSA under the same feed rate. However, in respect of product purity, the crossover of productivity between the two processes occurred near 99% H_2 purity. Also, the productivity of the seven-step PSA was significantly decreased near the 99.99% H_2 purity.

To understand the effects of the backfill step in detail, the H_2 concentration profiles of every step in gas phase at the end of each step are clearly shown in Fig. 4. A six-step PSA process had a dispersed wave front of H_2 after pressurizing the bed as shown in Fig. 4(a). The unfavorable wave front had a detrimental effect on the adsorption step because the mass transfer zone (MTZ) was very wide even at the adsorption step. However,

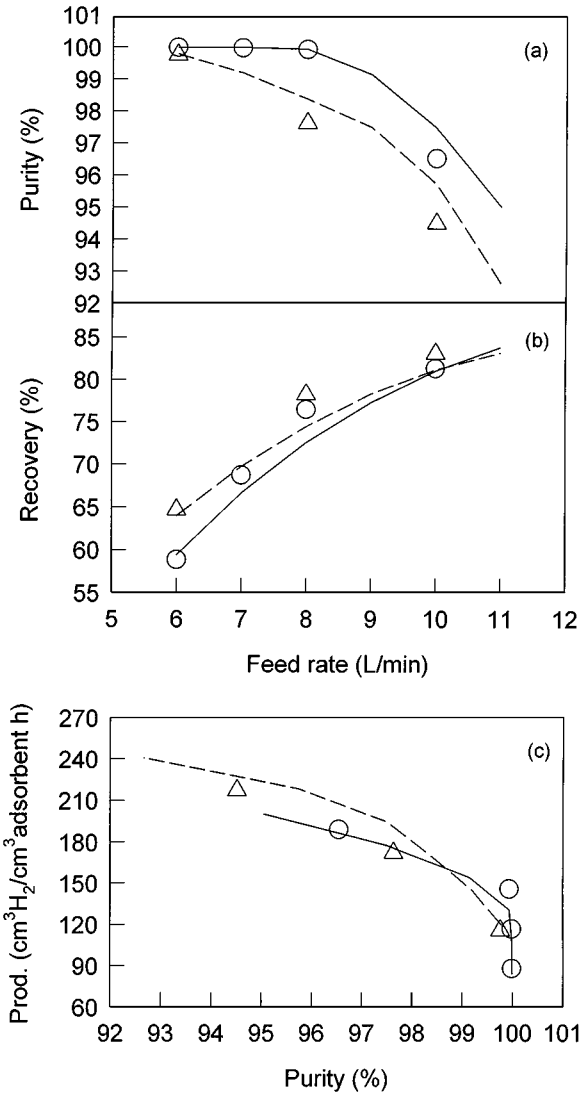

Figure 3. Comparison between a six-step process and a seven-step process at several feed rates under 11 atm adsorption pressure and 0.7 L/min purge rate using a layered bed with 0.35 carbon ratio (six-step process: – – – pred., △ expt.; seven-step process: — pred., ○ expt.).

in Fig. 4(b), the H_2 concentration profiles of the seven-step PSA process kept high purity at the product end section during all the steps of a cycle. Especially, the backfill step made the adsorption bed rich in H_2 and this led to a rather steep concentration wave front at the end of the feed pressurization step. This played a very important role in producing a high purity product because the contamination of the product end by strongly adsorbed components during the desorption steps had bad effects on the adsorption step of the next cycle. The importance of keeping the product end section

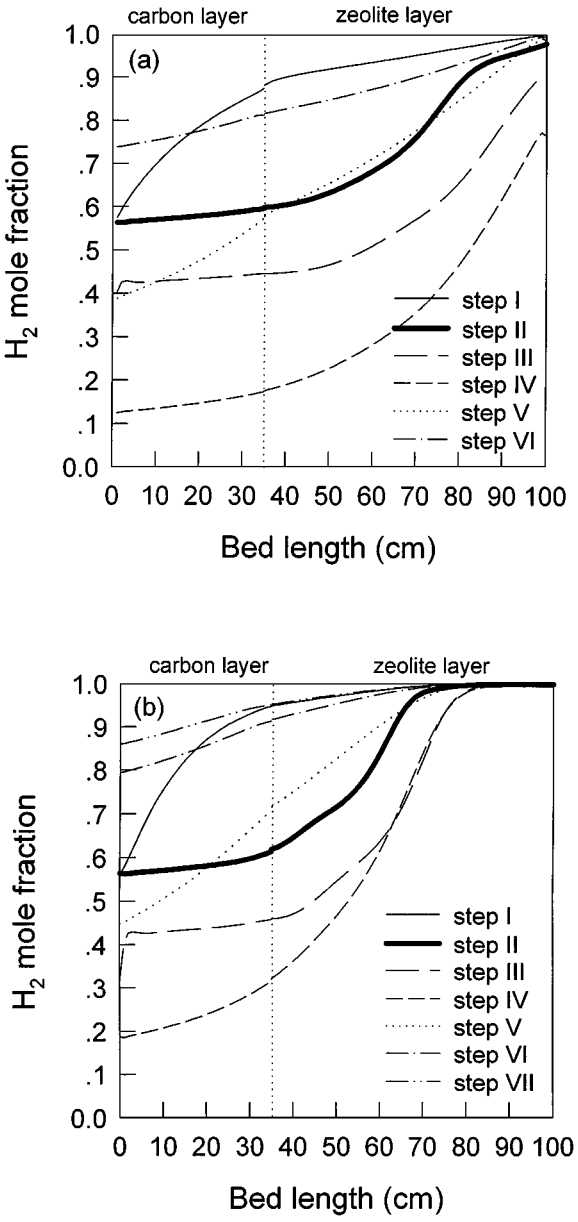

Figure 4. Concentration profiles of H_2 at the end of each step for (a) a six-step process and (b) a seven-step process at cyclic steady state under 11 atm adsorption pressure, 7 L/min feed rate and 0.7 L/min purge rate.

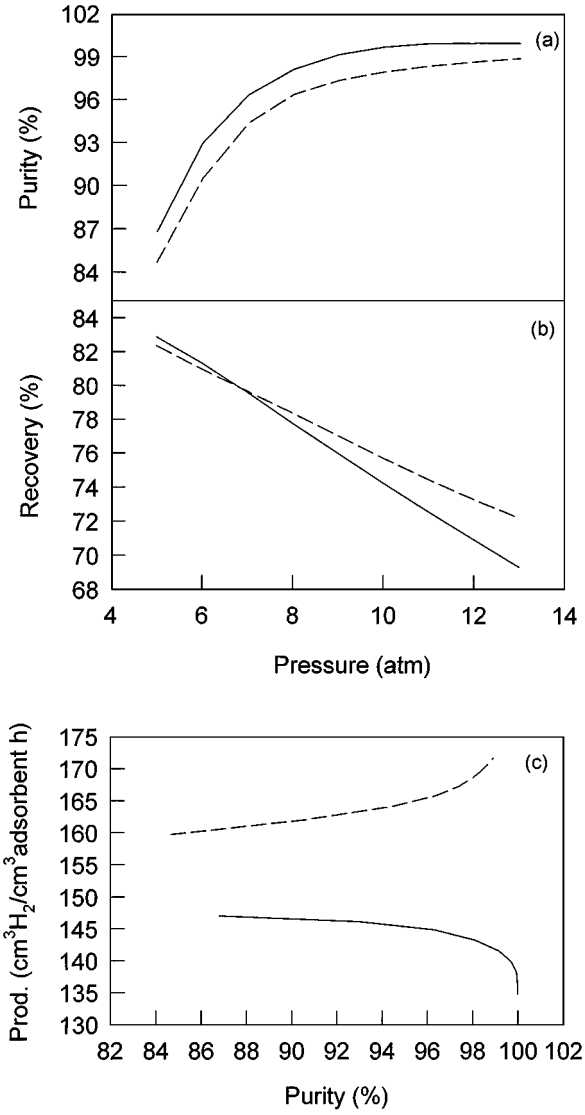

Figure 5. Effect of the adsorption pressure on product purity and recovery for six-step and seven-step processes under 8 L/min feed rate and 0.7 L/min purge rate. (six-step process: −−−. pred.; seven-step process: — pred.)

clean was also emphasized in other studies (Chou and Huang, 1994; Yang et al., 1997a). Judging from the concentration profiles at the end of the adsorption step in Fig. 4(b), a little more increase in the throughput by increasing the adsorption step time or using higher feed rate would not decrease product purity significantly as shown in Fig. 3.

The effect of the adsorption pressure in two PSA processes was investigated by a numerical simulation and the results are shown in Fig. 5. Over the full range of the adsorption pressure, the seven-step PSA process gave higher purity than the six-step PSA process, which showed a different trend from the results of purity in Fig. 3. However, recovery showed a similar trend with the effect of feed rate due to the same reason. In Fig. 5(c), the productivity of the six-step PSA was increased with an increase in the adsorption pressure,

while the productivity of the seven-step PSA was decreased with an increase in the adsorption pressure. In the case of the 6-step PSA process, the amount of raffinate at the pressurization step was proportional to the half of the adsorption pressure. However, the amount of raffinate at that step in the 7-step PSA process was proportional to the one-fourth of the adsorption pressure because of the backfill step. Therefore, the productivity in the 7-step PSA process decreased with an increase in the adsorption pressure because the increase in the raffinate with the adsorption pressure was smaller than the decrease in recovery. However, compared with the effect of feed rate in Fig. 3(c), the decrease in productivity by an increase in the adsorption pressure near the 99.99% H_2 purity was smaller than that by a decrease in the feed rate.

From the above results, a layered two-bed PSA process with a backfill step can be used to produce high purity H_2 (99.99+%) which can be obtained by employing a multi-bed H_2 PSA process using more than two beds (Yang, 1987; Ruthven et al., 1994; Rodrigues et al., 1989).

Comparison of Concentration and Temperature Profiles Among Three Different Beds

Since each step is affected by the previous step in a cyclic process, a basic study on the role of every step in a seven-step layered bed PSA process incorporating a backfill step is very important in understanding the performance of the process well. Then, based on the seven-step PSA process employed in this study, concentration and temperature profiles of selective key steps such as adsorption, pressure equilization, purge, and backfill steps at the cyclic steady state were presented to compare the layered bed with the activated carbon bed and zeolite 5A bed through Figs. 6–10. One velocity profile at each step in figures was also represented at the following step time: adsorption step (20 s), depressurizing pressure equilization step (2 s), purge step (20 s), pressurizing pressure equilization step (2 s), and backfill step (1 s). The velocity in a direction opposite to that of the feed was represented by a negative value.

Fig. 6 shows the corresponding profiles at the end of the adsorption step. It is very interesting that the concentration profiles are very similar to those of the breakthrough experiments obtained from Yang and Lee's work (Yang and Lee, 1998) despite its difference in initial conditions. The steep concentration wave fronts were formed by the compressive effect (Tondeur and Chlendi, 1993). This effect was prominent at the early stage of the adsorption step and counterbalanced the dispersive effect caused by mass transfer resistance and axial dispersion until the constant pattern of wave fronts were formed. On the other hand, the temperature profiles were different from those of the breakthrough experiments due to the influences of previous steps. The reason was that the temperature did not show a quick response to the ongoing steps like the gas concentration.

For two different single-adsorbent beds, all the wave concentration fronts began to form their own MTZ and move forward to the product end. However, they could not have their own distinctive MTZ because the adsorption bed was not long enough to separate every wave front as chromatography columns. As mentioned in the previous work (Yang and Lee, 1998), a well-known roll-up phenomenon was shown and this phenomenon affected the H_2 concentration profile. Since the adsorption capacity of N_2 on the activated carbon was less than that on zeolite 5A, N_2 became a major impurity in product stream of the activated carbon bed. However, the product stream of zeolite 5A bed contained lots of CO as well as N_2 due to dispersed and advanced wave front of CH_4. In addition, the sharp rise of temperature at the MTZ of CO_2 in zeolite 5A bed due to strong adsorption would lead to unsatisfactory performance. A layered bed with a different role at each layer could eliminate these disadvantages of two single-adsorbent beds because activated carbon adsorbed mainly CH_4 and zeolite 5A adsorbed CO and N_2. As a result, the temperature profile in this bed showed a slightly faster increase and decrease in each layer than that in single-adsorbent beds.

The evolution and the role of the depressurizing pressure equalization step are shown in Fig. 7. At this step, every concentration wave front and temperature profile moved further toward the product end without any conspicuous change in the shapes of wave fronts. However, owing to the desorption by the decrease in total pressure, the strong adsorbates were desorbed and diffused out, making the mole fractions of CH_4, CO, CO_2, and N_2 increase and making that of H_2 decrease. Although the compressive effect was not so great like the case of the adsorption step because of the increase in mole fraction in the desorption zone, the compressive effect from isotherm curvature was also applied to this step. On the other hand, velocity increased rapidly from zero

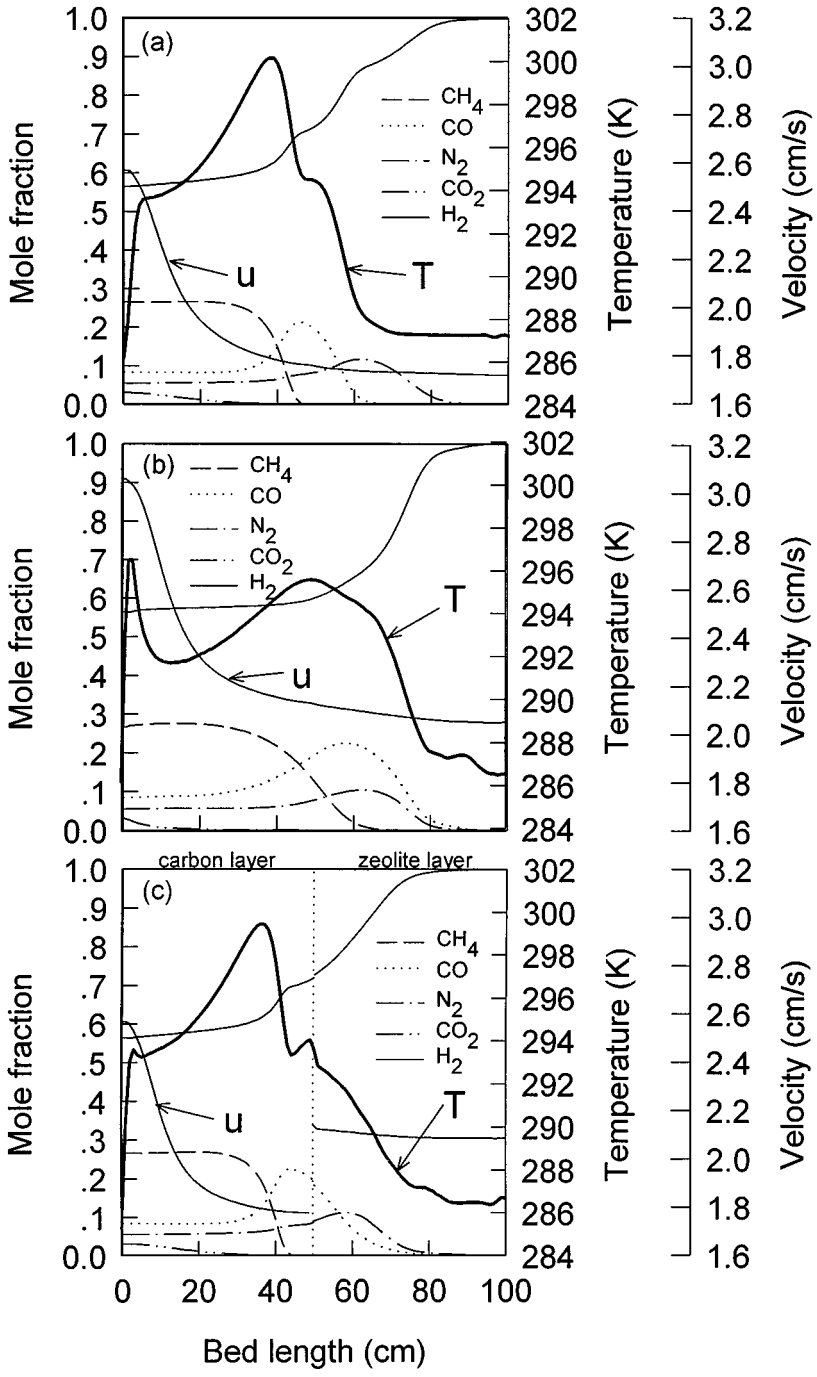

Figure 6. Concentration, temperature, and velocity (20 s) profiles at the end of the adsorption step at a cyclic steady state for (a) activated carbon bed, (b) zeolite 5A bed, and (c) layered bed (c.r. = 0.5) processes under 10 atm adsorption pressure, 7 L/min feed rate and 0.7 L/min purge rate.

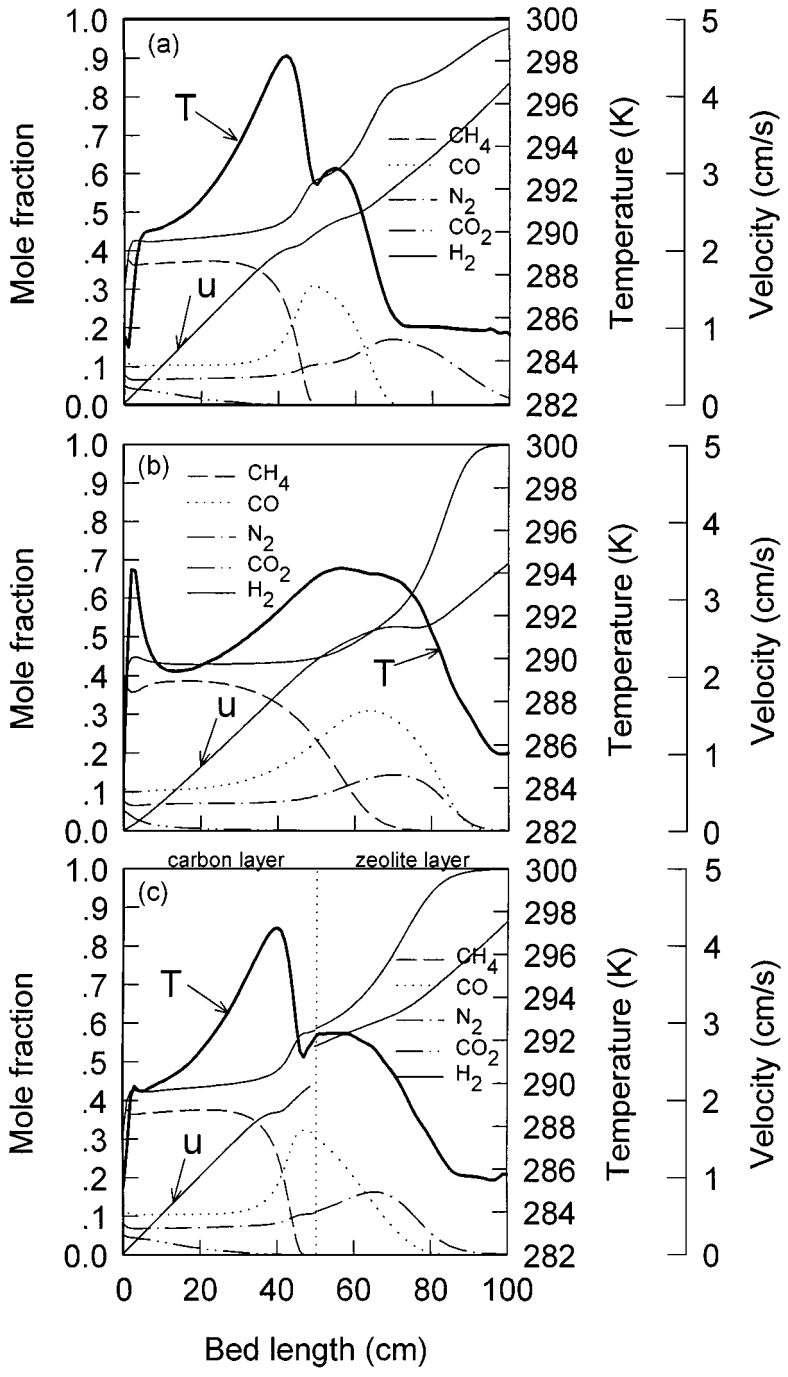

Figure 7. Concentration, temperature, and velocity (2 s) profiles at the end of depressurizing pressure equalization step at a cyclic steady state for (a) activated carbon bed, (b) zeolite 5A bed, and (c) layered bed (c.r. = 0.5) processes under 10 atm adsorption pressure, 7 L/min feed rate and 0.7 L/min purge rate.

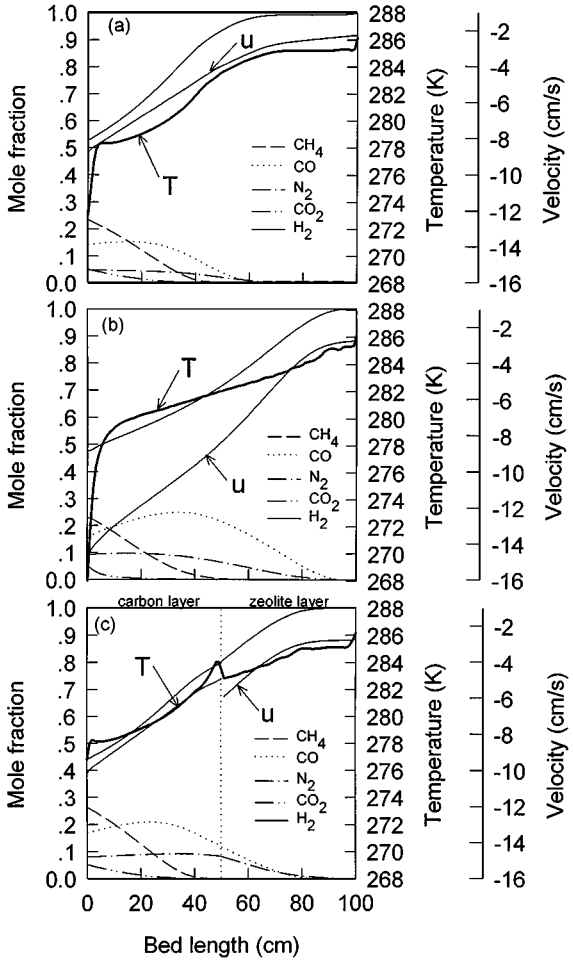

Figure 8. Concentration, temperature, and velocity (20 s) profiles at the end of a purge step at a cyclic steady state for (a) activated carbon bed, (b) zeolite 5A bed, and (c) layered bed (c.r. = 0.5) processes under 10 atm adsorption pressure, 7 L/min feed rate and 0.7 L/min purge rate.

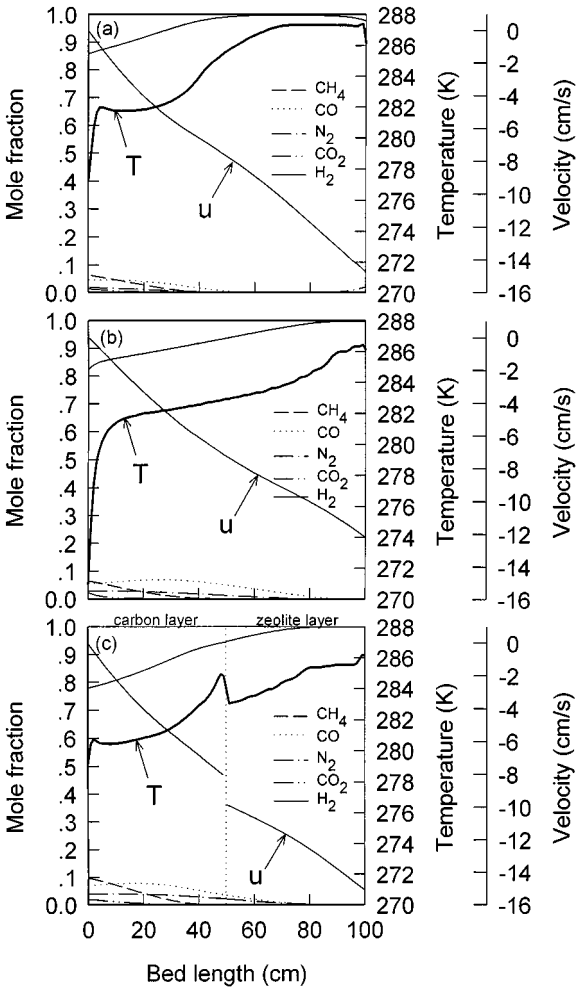

Figure 9. Concentration, temperature, and velocity (2 s) profiles at the end of a pressurizing pressure equalization step at a cyclic steady state for (a) activated carbon bed, (b) zeolite 5A bed, and (c) layered bed (c.r. = 0.5) processes under 10 atm adsorption pressure, 7 L/min feed rate and 0.7 L/min purge rate.

at the closed end to the fastest velocity at the open end mainly due to fluid dynamic effect. As a result, the behavior of concentration wave fronts during the DPE step depended on the relative importance of two antagonistic effects. The overall effect, however, made the wave fronts dispersive because the effect of velocity was stronger than that of the isotherm curvature.

It is noteworthy that, for the activated carbon bed process, N_2 wave front propagates fast, resulting in the early breakthrough of N_2. This phenomenon will give a negative effect on product purity because the activated carbon can treat N_2 less than zeolite 5A. Note that the DPE should not make the wave fronts be dispersed at the downstream part of the adsorption bed which determines the breakthrough. In this respect, the activated carbon bed was unfavorable because the N_2 wave front in the bed propagated so fast that the product end section was contaminated with N_2 in comparison with other beds.

For optimum regeneration of the bed, the H_2 concentration of the feed end should be the same as that of the feed concentration before the pressurization or backfill step is initiated (Liow and Kenney, 1990). This suggests that the use of a purge step at the end of the depressurization step would enhance product purity and recovery. As shown in Fig. 8, the purge step had the same effect as the countercurrent depressurization

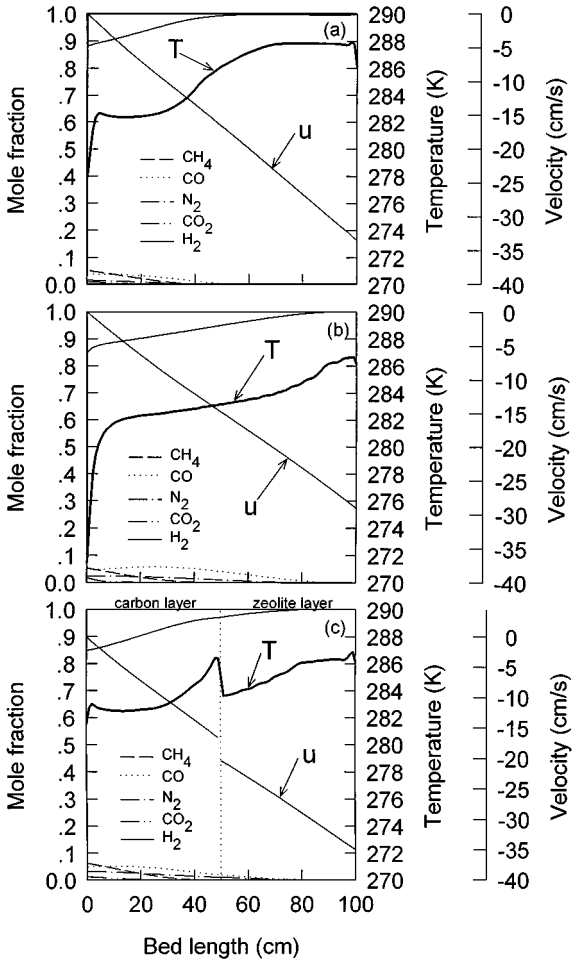

Figure 10. Concentration, temperature, and velocity (1 s) profiles at the end of a backfill step at a cyclic steady state for (a) activated carbon bed, (b) zeolite 5A bed, and (c) layered bed (c.r. = 0.5) processes under 10 atm adsorption pressure, 7 L/min feed rate and 0.7 L/min purge rate.

step on concentration wave fronts, namely a dispersive effect. Because of the intrinsic dispersive effect at this step (Yang et al., 1998), all the wave concentration fronts spread out as they moved backward. The velocity distribution increased toward the open end. Both higher velocity and concentration of the strong adsorbates at the feed end led to a synergistic dispersive effect of wave front, smoothing out the stepwise change of H_2 concentration profiles. The light product from the product end desorbed strong adsorbates out of the adsorption bed because this step made the partial pressure of strong adsorbates decrease. The H_2 concentration became rich in large extent compared with the corresponding profiles of the previous step. It is noteworthy that the purge step has the greatest effect on the activated carbon bed, especially, at the product end. This means that the activated carbon can easily be regenerated because of the relatively weak adsorption of the adsorbates on the surface. The temperature continued to go down because of the endothermic heat of desorption. On the other hand, the zeolite 5A bed still maintained widely dispersed concentration fronts and the layered bed showed an intermediate behavior of two single-adsorbent beds.

After the pressurizing pressure equalization step, the H_2 mole fraction increased in large extent as shown in Fig. 9. Because of the increase in total pressure, many adsorbates were adsorbed and these mole fractions were reduced at the gas phase. However, from the concentration profiles of H_2 and N_2 for the activated carbon bed, as shown in Fig. 9(a), it was found that some N_2 remained in the product end. This can be explained by the concentration profiles of the depressurizing pressure equalization step (Fig. 7(a)). When the activated carbon bed was used, the N_2 breakthrough occurred at the DPE step and the impure stream containing N_2 moved into the product end of the other bed undergoing a PPE step. Therefore, if N_2 was not treated in a reasonable way before the adsorption step, product purity would not be very high. The product end of a zeolite bed remained cleaner than that of the activated carbon bed, while the concentration profile of CO was widely dispersed in the bed. However, the product end of a layered bed remained cleaner than that of any other bed as shown in Fig. 9(c). Since the impurities in the gas stream were adsorbed in the activated carbon near the layer interface, a small temperature excursion occurred at the interface.

The purpose of pressurizing the adsorption bed further with a light product was to make the product end section purer as shown in Fig. 10. Then, the effect of a backfill step would be an additional purge. If the recompression gas is rich in adsorbable components, the operation should be carried out cocurrently. However, a pure inert gas should always be introduced at the product end. Comparing Fig. 5 (feed pressurization step) with Fig. 10, the role of a backfill step was not clearly seen. Since this step improved purity at a high purity level, only a slight increase of H_2 mole fraction was found. However, the zeolite bed still had the dispersed wave fronts like a PPE step and the product end of the activated carbon bed was also contaminated by a small amount of N_2 which stemmed from the previous step. It gave negative effect on the adsorption step to obtain high purity product. The temperature profile of a single-adsorbent bed did not change much from the previous

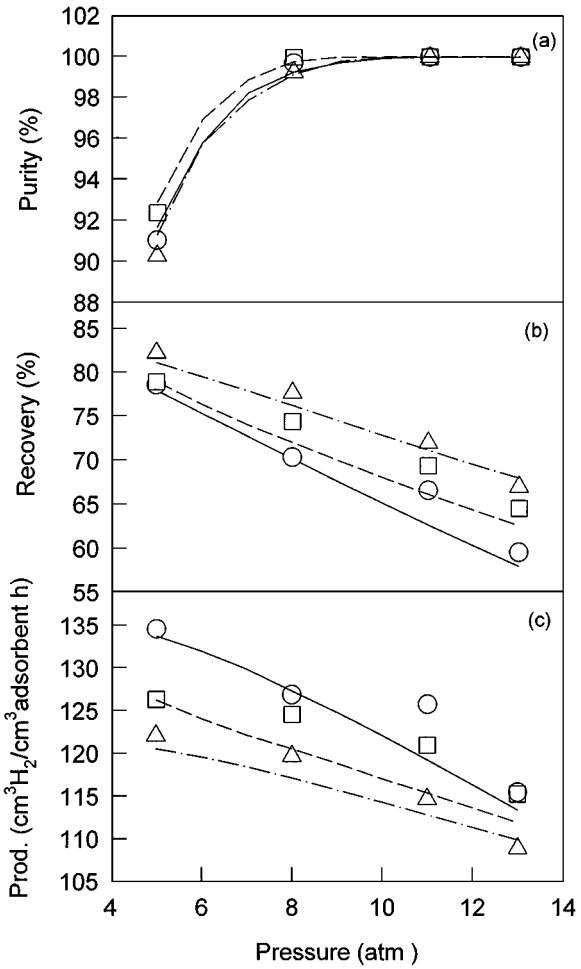

Figure 11. Effect of adsorption pressure on (a) purity and (b) recovery for activated carbon bed, zeolite bed, and layered bed (c.r. = 0.5) processes under 7 L/min feed rate and 0.7 L/min purge rate (activated carbon bed: — pred., ○ expt.; layered bed: – – – – pred., □ expt.; zeolite bed: –·–·– pred., △ expt.)

step, while the temperature excursion near the interface of the layered bed became slightly larger than that of the previous step due to the readsorption of adsorbates desorbing from the zeolite layer.

In summary, N_2 became a major product impurity in the activated carbon bed, while the product of zeolite 5A bed contained CO as well as N_2 due to the dispersive wave front of CH_4. As shown in the concentration and temperature profiles at each step, the layered bed combined the characteristics of the activated carbon bed and zeolite 5A bed to treat the impurities. As a result, the layered bed was expected to obtain higher purity of H_2 than the other beds and the experimental results would verify this simulated results in the following section.

Effect of Adsorption Pressure on PSA Processes

A comparison was made of the effects of the adsorption pressure on the seven-step two-bed PSA process using two single-adsorbent beds and a layered bed with 0.5 carbon ratio in Fig. 11. The overall trends of purity variation with adsorption pressures did not show any great difference among three kinds of adsorption beds. The H_2 purity declined significantly at low pressure and there was no remarkable variation in product purity above around 11 atm at which a commercial H_2 PSA process using four adsorption beds has been operated for the recovery of high purity hydrogen (99.99+%) from COG. In the case of the single-adsorbent PSA processes, purity dropped rapidly below 11 atm, while H_2 purity for the layered bed PSA process with 0.5 carbon ratio decreased slowly even below 11 atm.

Figure 11(b) also shows that H_2 recovery drops almost linearly with the adsorption pressure for all types of adsorption beds. This was because the amount of H_2 loss from the feed end during a countercurrent depressurization step was proportional to the adsorption pressure or, more accurately speaking, to the pressure of the pressure equalization step. Unlike the case of H_2 purity, zeolite 5A bed was the best in respect of recovery and the activated carbon bed gave the lowest recovery. This implied that higher recovery could be expected in a layered bed process with an increase in a zeolite 5A layer. However, due to the difference in purity, the result of productivity turned out to be opposite to that of recovery and the difference in productivity among three different processes decreased with an increase in the adsorption pressure as shown in Fig. 11(c). The productivity of the layered bed showed an intermediate value between that of the activated carbon bed and that of the zeolite 5A bed like the result of recovery.

However, it is noteworthy that the layered bed gives higher product purity than two single-adsorbent beds at the same operating condition as explained in the simulated result. Even near 11 atm the adsorption pressure which is typically operated in steel industry, the product purity in zeolite 5A and in the activated carbon PSA processes was less than 99.99%, while that in the layered bed PSA process was 99.99+%. Moreover, as shown in Table 2, at similar recovery in the range of high purity, the layered bed gives higher product purity than two single-adsorbent beds. This implies that the optimum packing ratio for purity is present because the two single-adsorbent PSA processes are inferior to the layered bed PSA over a full range of the operating conditions.

Table 2. Comparison between performance in the layered bed process and the single-adsorbent bed processes under various operating conditions.

	Activated carbon bed		Layered bed (c.r. = 0.5)		Zeolite 5A bed	
Unit	Purity	Recovery	Purity	Recovery	Purity	Recovery
Adsorption pressure (feed rate: 7 LSTP/min, purge rate: 0.7 LSTP/min)						
5	91.641 (91.022)	77.888 (78.54)	92.841 (92.343)	78.901 (78.89)	91.281 (90.256)	81.066 (82.19)
8	99.216 (99.675)	70.127 (70.32)	99.742 (99.955)	71.982 (74.35)	99.104 (99.224)	76.186 (77.63)
11	99.978 (99.988)	62.665 (66.62)	99.999 (99.991)	66.154 (69.38)	99.986 (99.983)	71.129 (71.96)
13	99.999 (99.993)	57.982 (59.61)	100.000 (99.997)	62.621 (64.58)	99.992 (99.993)	68.028 (67.03)
Feed rate (adsorption pressure: 11 atm, purge rate: 0.7 LSTP/min)						
6	99.998	57.248	99.999	61.314	99.987	65.853
7	99.901	65.112	99.989	68.034	99.968	72.779
8	99.415	71.179	99.765	73.426	99.017	78.057
9	98.309	76.006	98.672	77.643	97.015	81.850
Purge rate (adsorption pressure: 11 atm, feed rate: 7 LSTP/min)						
0.5	99.551	69.791	99.789	72.636	99.246	77.791
0.8	99.957	62.795	99.999	65.781	99.985	70.263
0.9	99.979	60.501	99.999	63.547	99.984	67.807
1.0	99.990	58.220	99.999	61.343	99.987	65.363

*Parenthesis represents the experimental data (unit: %).
Adsorption pressure in atm, feed rate and purge rate in LSTP/min.

Conclusions

A two-bed PSA process for recovering H_2 from COG was studied experimentally and theoretically by using two different single-adsorbent beds and a layered bed packed with activated carbon and zeolite 5A.

In the layered bed PSA process, incorporating a backfill step after the pressurizing pressure equalization step resulted in an increase in product purity with a decrease in recovery. The purity difference between two processes with/without a backfill step increased with the feed rate, while the recovery difference decreased. However, the change in purity difference became small with the change in adsorption pressure, while the recovery difference increased with the adsorption pressure. This means that the backfill step can be a viable alternative for an increase in product purity without increasing the number of the adsorption bed.

The mathematical model proposed successfully predicted the steady-state behavior of the PSA processes with/without the backfill cycle and showed the role of each individual step. The predicted concentration and temperature profiles inside the adsorption beds showed that the product end in the activated carbon bed was contaminated by N_2 and the concentration wave fronts of CO and N_2 were widely dispersed in the zeolite 5A bed. As a result, it was very hard to obtain higher than 99.99+% H_2 purity product from COG through single-adsorbent PSA processes even by applying the backfill step. However, the layered bed reduced the disadvantages caused by two different single-adsorbent beds and gave experimentally and numerically best purity at constant recovery in the range of high product purity.

From the effect of the adsorption pressure on the PSA process performance using single-adsorbent or layered beds, it was found that the product purity of a layered bed was not between the limits of two single-adsorbent bed processes. As found in the comparison of the simulated dynamics of each step in three different PSA processes, it indicated that the synergistic effects of two adsorbents occurred. Unlike the case of purity, the recovery and productivity of a layered bed process was between the limits of two single-adsorbent bed processes.

Nomenclature

A Cross sectional area, m^2
B Langmuir-Freundlich isotherm parameter, atm^{-1}

C_p Heat capacity, J/(kg K)
D_L Mass axial dispersion coefficient, m^2/s
h Heat transfer coefficient, J/(m^2 s K)
K_L Effective axial thermal conductivity, J/(m s K)
k_g Thermal conductivity of fluid, J/(m s K)
k_s Thermal conductivity of particle, J/(m s K)
n Langmuir-Freundlich isotherm parameter
P Pressure, atm
Pr Prandtl number, $(C_p)_g \mu / k_g$
q_m Langmuir-Freundlich isotherm parameter, mol/kg
$\bar{q}$ Volume-averaged adsorbed phase concentration, mol/kg
q^* Equilibrium adsorbed phase concentration, mol/kg
Q Average isosteric heat of adsorption, J/mol
R Radius, m
Re Reynolds number, $\rho_g v(2R_p)/\mu$
Sc Schmidt number, $\mu \rho_g / D_m$
t Time, s
T Solid phase and gas phase temperature, K
T_{atm} Ambient temperature, K
t_s Stoichiometric breakthrough time, s
u Interstitial velocity, m/s
y Mole fraction in gas phase
z Axial position in a adsorption bed, m
α Total void fraction
δ, ϕ Parameters used in Eq. 9
ε Interparticle void fraction
μ Viscosity, (m/kg s)
v Superficial velocity, m/s
ρ Density, m^3/kg
ω LDF coefficient, s^{-1}

Subscripts

B Bed
i Component i
p Pellet
g Gas phase
s Solid phase
w Wall

Acknowledgment

The financial assistance and support of Sunkyong Engineering & Construction Limited and R&D Management Center for Energy and Resources are gratefully acknowledged.

References

Alpay, E., C.N. Kenney, and D.M. Scott, "Simulation of Rapid Pressure Swing Adsorption and Reaction Processes," *Chem. Eng. Sci.*, **48**, 3173–3186 (1993).

Chou, C.-T. and W.-C. Huang, "Simulation of a Four-Bed Pressure Swing Adsorption Process for Oxygen Enrichment," *Ind. Eng. Chem. Res.*, **33**, 1250–1258 (1994).

Hartzog, D.G. and S. Sircar, "Sensitivity of PSA Processes Performance to Input Variables," *Adsorption*, **1**, 133–151 (1995).

Kirkby, N.F. and C.N. Kenney, "The Role of Process Steps in Pressure Swing Adsorption," *Fundamentals of Adsorption*, pp. 319–326, Engineering Foundation, New York, 1987.

Kumar, R., V.G. Fox, D.G. Hartzog, R.E. Larson, Y.C. Chen, P.A. Houghton, and T. Naheiri, "A Versatile Process Simulator for Adsorptive Separations," *Chem. Eng. Sci.*, **49**, 3115–3125 (1994).

Liow, J.-L. and C.N. Kenney, "The Backfill Cycle of the Pressure Swing Adsorption Process," *AIChE J.*, **36**, 53–65 (1990).

Lu, Z.P., J.M. Loureiro, A.E. Rodrigues, and M.D. LeVan, "Pressurization and Blowdown of Adsorption Beds-II. Effect of the Momentum and Equilibrium Relations on Isothermal Operations," *Chem. Eng. Sci.*, **48**, 1699–1707 (1993).

Rodrigues, A.E., M.D. LeVan, and D. Tondeur, *Adsorption: Science and Technology*, Kluwer Academic Publishers, Boston, 1989.

Ruthven, D.M., S. Farooq, and K.S. Knaebel, *Pressure Swing Adsorption*, VCH Publishers, New York, 1994.

Skarstrom, C.W., "Heatless Fractionation of Gaseous Materials," U.S. Patent 3104162, 1963.

Suzuki, M., *Adsorption Engineering*, Elsevier, Amsterdam, 1990.

Wakao, N. and T. Funazkri, "Effect of Fluid Dispersion Coefficients on Particle-to-Fluid Mass Transfer Coefficients in Packed Beds," *Chem. Eng. Sci.*, **33**, 1375–1384 (1978).

Tondeur, D. and M. Chlendi, "Front Analysis and Cycle Policy in PSA Operations," *Gas Sepa. Purif.*, **7**, 105–109 (1993).

Yang, R.T., *Gas Separation by Adsorption Processes*, Butterworths, Boston, 1987.

Yang, J., H. Ahn, H. Lee, and C.-H. Lee, "Hydrogen Recovery from Coke Oven Gas Using a Layered-Column PSA Porcess," *Fundamentals of Adsorption*, pp. 897–902, Elsevier, 1998.

Yang, J., J.-W. Chang, and C.-H. Lee, "Separations of Hydrogen Mixtures by a Two-Bed Pressure Swing Adsorption Process Using Zeolite 5A," *Ind. Eng. Chem. Res.*, **36**, 2789–2798 (1997a).

Yang, J., C. Cho, K.H. Baek, and C.-H. Lee, "Comparison of One-Bed and Two-Bed H_2 PSA Using Zeolite 5A," *HWAHAK KONGHAK*, **35**, 545–551 (1997b).

Yang, J. and C.-H. Lee, "Adsorption Dynamics of a Layered Bed PSA for H_2 Recovery from Coke Oven Gas," *AIChE J.*, **44**, 1325–1334 (1998).

Yang, J., M.-W. Park, J.W. Chang, S.-M. Ko, and C.-H. Lee, "Effects of Pressure Drop in a PSA Process," *Korean J. Chem. Eng.*, **15**, 211–216 (1998).